Design study for International Thermonuclear Experimental Reactor high resolution x-ray spectroscopy array

R. Barnsley[a)]
Euratom/UKAEA Fusion Assoc., Culham Science Centre, Abingdon, OX14 3DB, United Kingdom and Department of Pure and Applied Physics, Queens University, Belfast, BT7 1NN, United Kingdom

M. O'Mullane
Department of Physics and Applied Physics, University of Strathclyde, Glasgow, G4 0NG, United Kingdom

L. C. Ingesson
EFDA Close Support Unit-Garching, Boltzmannstr. 2, D-85748 Garching, Germany

A. Malaquias
Associação Euratom/IST, CFN, Av. Rovisco Pais, 1049-001 Lisboa, Portugal

(Presented on 20 April 2004; published 6 October 2004)

The impurity line and continuum emission for International Thermonuclear Experimental Reactor (ITER) reference H-mode and Internal Transport Barrier (ITB) plasmas were modeled using the SANCO impurity transport code. Using the instrument sensitivity for a spatially resolving crystal spectrometer array with doubly-curved crystals and two-dimensional detectors, signals, and signal-to-noise ratios were calculated for impurities including argon, iron, and krypton. These were shown to have lines suitable for the measurement of the ion temperature (0.5–30 keV) and the rotation over almost the entire plasma minor radius. The main contribution to the signal-to-noise is the plasma continuum radiation on which the lines are superimposed. The tolerable impurity concentration is limited by the incremental radiated power ΔP_{rad}, there being a broad operating range between about 100 kW and 10 MW. The spectrometer array has now been integrated into the ITER design. A quasitomographic technique to reconstruct the T_i and rotation profiles, is reported by Ingesson *et al.* [C. Ingesson, these proceedings]. © *2004 American Institute of Physics.* [DOI: 10.1063/1.1790044]

I. EMISSION MODELING

International Thermonuclear Experimental Reactor (ITER) H-mode and Internal Transport Barrier (ITB) plasmas were modelled with the Atomic Data and Analysis Structure (ADAS),[2] and the SANCO[3] impurity transport code, using the radial profiles[4] of T_i, T_c, and n_e shown in Fig. 1. All the results for H-mode and ITB plasmas are similar, and only the H-mode data are presented here. The main constraint on the allowable added impurity concentration is not the increase in Z_{eff}, which is very small, but the additional radiated power, ΔP_{rad}. The incremental radiated powers for added impurity concentrations of $10^{-5}.n_e$ are for Ar 0.25 MW, for Fe 0.8 MW, and for Kr 1.4 MW. The radial profiles of ΔP_{rad} are strongly weighted toward the outer plasma, and while the added impurity is inefficient to the extent that most of the ΔP_{rad} is not in the observed lines, radiative losses from the core are very low.

The free-free and free-bound continuum emission was also modeled, as it is relatively much stronger on ITER than existing tokamaks and, for a well-shielded detector, is the major source of noise on the T_i and rotation measurements. This is particularly true for krypton, where the radiated power is shared over more ionization stages, and for a given ΔP_{rad} the line/continuum ratio is lowest. Line-to-continuum ratios range from ~1 for Kr^{34+} in the core, to ~30 for Ar^{16+} near the edge.

There is considerable overlap in the suitability of the various emission profiles (Fig. 2), but generally, Kr^{34+}, Kr^{35+}, and Fe^{25+}, with broad emission profiles peaked toward the core, are best suited for core measurements. Broad, slightly hollow emission profiles that are problematic for a single-chord system pose no major problem for a continuously space-resolved system, provided the signal-to-noise ratio is good enough to reconstruct the profiles. Better suited for the outer plasma, with hollow profiles and strong edge emission, are Fe^{24+}, Ar^{16+}, and Ar^{17+}.

II. DESIGN INTEGRATION

There is widespread effort to demonstrate space-resolving high-resolution x-ray spectrometers using doubly curved crystals and two-dimensional detectors, for measurements of ion temperature and plasma rotation,[5–9] and to measure the spectrum of He-like Kr,[10,11] the primary candidate for such measurements on ITER. The system described here has evolved from the ITER-98 design.[12,13] Due to the long, narrow equatorial port plugs on ITER-98, a wide direct view of the plasma was impossible, and all poloidal spatial views except the central chord were achieved with graphite reflectors. In the present design, multiple imaging crystal spec-

a)Electronic mail: RB@JET.UK

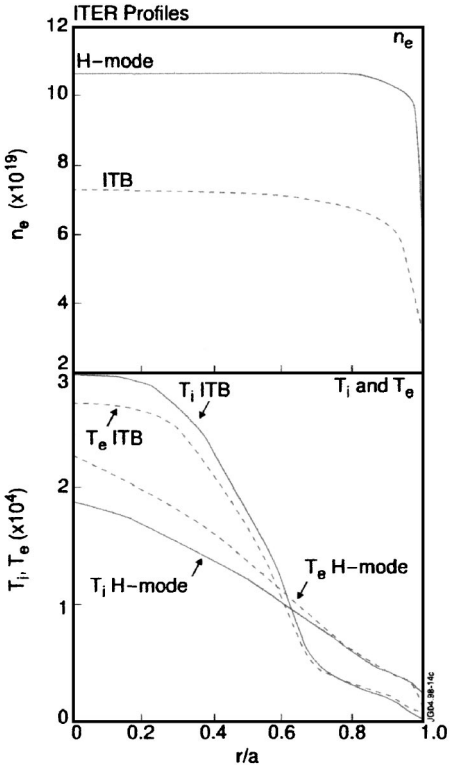

FIG. 1. Radial profiles of n_e, T_e, and T_i for ITER H-mode and ITB plasmas, used for emission simulations.

trometers are located in upper and equatorial ports (Figs. 3 and 4). The shorter equatorial port of ITER, and the upper port, together allow direct views of most of the plasma minor radius. The region $\sim 0.7 < r/a < \sim 0.9$ is inaccessible directly, and is viewed by two or more graphite reflectors, shown here in an upper port, though equally feasible in an equatorial port. Graphite has typical peak reflectivity of 30% and a bandpass of ~1%, with a further disadvantage that the

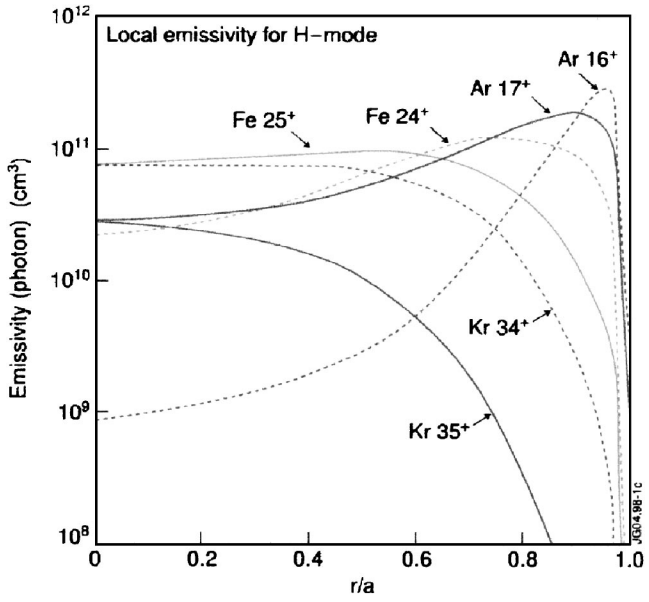

FIG. 2. Local emissivity for H- and He-like Ar, Fe, and Kr ions at $\Delta P_{\text{rad}} = 500$ kW in each case. There is good emission over the whole plasma, suitable for T_i and rotation measurements.

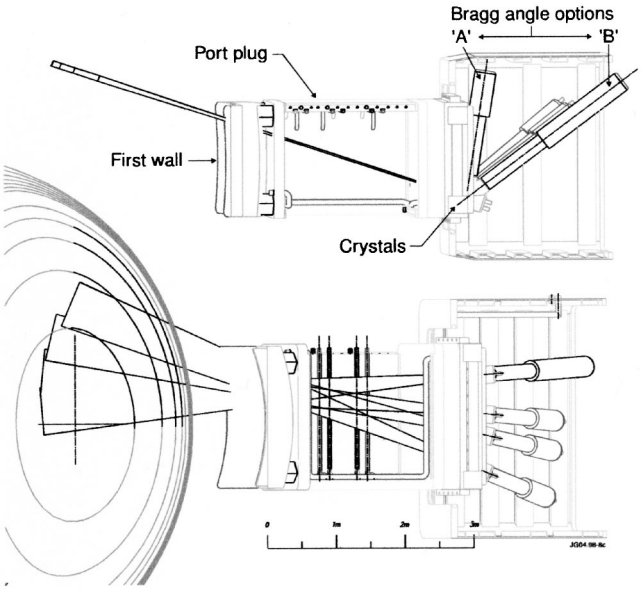

FIG. 3. Schematic of the equatorial port array of imaging spectrometers.

reflection angles built into the port-plug must be carefully selected for specific wavelengths. The alternative of locating the spectrometers inside the port plug has been avoided on grounds of reduced access and increased background.

Various options for toroidal view and detector location have been designed. Figure 3 shows the maximum practical equatorial toroidal view of 18.5°. A spherical crystal requires a Bragg angle of ~50° ("A" in Fig. 3) which, within the space behind the port-plug, implies a crystal-detector distance of 1.5 m, crystal radius of 2 m, and port-detector distance less than 0.5 m. The virtual entrance slit is about half way down the port-plug. A toroidal crystal at ~30° Bragg angle ("B" in Fig. 3), may have poorer off-axis imaging, but otherwise has several advantages. The port-detector distance of 2.3 m facilitates detector shielding and access, while detector-crystal distance of 2.5 m implies a primary crystal radius of 5.3 m, and improves input shielding by placing the

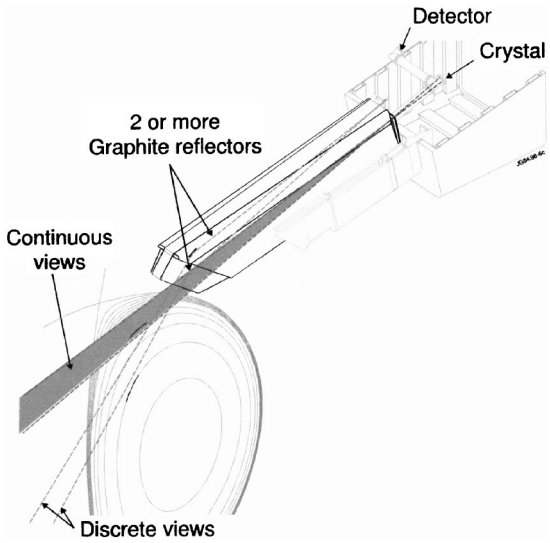

FIG. 4. Schematic of the imaging x-ray crystal spectrometer, and discrete-chord graphite reflectors, in an upper port.

virtual entrance slit closer to the blanket penetration. For both options, an asymmetric crystal cut could place the virtual slit much closer to the blanket penetration. Both options require a conical slot in the port-plug for optimum input shielding, this effect being less for option "B." The reduced angular dispersion of "B" is balanced by its longer detector arm, so that the required detector resolution for $\lambda/\delta\lambda = 10\,000$ is about 0.25 mm in both cases.

The total required detector height of ~800 mm is determined by the demagnification of ~0.2, and is independent of the number of crystals used to cover the total viewing angle. About five individual detectors are required, with a height of 150–200 mm in the imaging direction, with a spatial resolution of ~5 mm, allowing >100 resolvable chords. In the λ-direction, a width of ~50 mm with resolution of 0.1–0.25 mm is required. The peak count-rate density is $\sim 10^7$ count/cm^2 s with an average of 10^6 count/cm^2 s. For signal-to-noise estimates, we have assumed a n-γ background count density of 10^5 count/cm^2 s, based on an unshielded flux of 10^7 n-γ/cm^2 s and an attenuation factor of 100, due to a shield transmission of 10% and detector sensitivity of 10%. This is a conservative estimate compared to (JET) where, as discussed below, a background attenuation of 10^6 was achieved. The required performance is typical of detectors in use or in development for high-flux sources such as synchrotrons. These include gas-microstructure proportional counters and solid-state arrays with individual pulse processing chain for each pixel.

III. SENSITIVITY

The count-rate N'(count/s) from a spectral line with intensity I (photon/cm^2 s), is $N' = I.S$ where, for a Johann spectrometer, $S = P_{gr}.\kappa.\psi.R_c.h_x.h_y.\eta/4\pi$, with the peak reflectivity of any graphite prereflector P_{gr}, crystal filling-factor κ ($\kappa = 1$ with suitable input geometry), vertical divergence ψ (rad), crystal reflection integral R_c (rad), crystal projected area $h_x.h_y$, and combined window/detector efficiency η. For a total vertical divergence ψ_{tot}, divided into n_{ch} viewing channels, the vertical divergence per channel is $\psi_{ch} = \psi_{tot}/n_{ch}$.

Sensitivities are based on a Graphite(002/004)-Ge(220/440) system at Bragg angles $\theta_{Gr} \sim 16°$ and $\theta_{Ge} \sim 28°$, observing the Fe lines around 0.18 nm in first order and the Kr lines around 0.095 nm in second order. Taking $\psi_{tot} \sim 0.5$ rad, $n_{ch} = 35$, crystal aperture $h_x.h_y = 5 \times 5$ cm^2, and $\eta = 0.5$, the sensitivities for Fe and Kr, without and with graphite reflectors are, respectively, $S_{Fe} = 9.4$, $S_{Fe,Gr} = 2.8$, $S_{Kr} = 1.3$ and $S_{Kr,Gr} = 0.25 \times 10^{-7}$ cm^2. The different diffraction orders will be discriminated by the detector energy resolution. Sensitivities for spherical crystals, at Bragg angles close to 50°, are similar to those used here.

IV. BACKGROUND RADIATION

Neutron scattering has been modeled[14] for the upper port system. The flux of neutrons of energy $E > 0.1$ MeV is 3.10^9 n/cm^2 s at the crystal (Fig. 4) and 3.10^7 n/cm^2 s at the detector location, with no additional shielding behind the port-plug.

There are two sources of detector background; first, scattering along the optical path into the detector of the direct flux incident on the crystal, and second, the general background at the detector due to secondary scattering, incomplete shielding by the port-plug, and other port penetrations. Background measurements during (D-T) experiments on the Joint European Torus (JET) have enabled these two noise sources to be quantified and largely isolated from each other.

The JET double-crystal spatially scanning spectrometer[15] was inside the torus hall, mounted to an upper port, with its 12 mm deep Ar-filled detector shielded by 0.1 m of Pb surrounded by 1 m of borated polyethylene. The two-reflection optics prevented a direct line of sight from the detector to either the plasma or the first crystal, so that transmission through the shield was the main source of detector background. In the JET preliminary tritium experiment (PTE-1991), background in the detector was 100 count/cm^2 s, for an estimated neutron flux of 10^8 n/cm^2 s outside the detector shield, representing an effective attenuation factor of 10^6.

The JET Bragg survey spectrometer,[16] located on an 18 m vacuum beam-line[17] outside the JET 3 m concrete bioshield, has its 4 mm deep, Ar-filled low-energy detector only 50 mm from the plasma-facing crystal. In the JET deuterium-tritium experiment of 1997, the background in this detector was 1000 count/cm^2 s for a direct neutron flux into the instrument of 10^9 n/s. Some fraction of that background was due to secondary scattering within the spectrometer bunker, so the effective attenuation factor of 10^6 represents a lower limit.

Together, these results show that the background count-rate due to scattering of direct n-γ flux from crystal into detector is very low, and that a gas-filled detector can be well shielded from indirect background radiation at levels predicted behind an ITER port-plug. Similar results for vacuum ultraviolet/extreme ultraviolet spectrometers with microchannel-plate detectors are presented in these proceedings by Coffey.[18]

V. SIMULATED SIGNALS

Figure 5 shows the simulated count-rate per chord, for 35 chords, for the principal emission lines of H- and He-like ions of Ar, Fe, and Kr, namely, $1s$-$2p$ Lyα_1, and the $1s^2$-$1s2p$ "w" line.

Given the lower radiation efficiency and lower spectrometer sensitivity for Kr^{34+} compared to Fe^{25+}, the ΔP_{rad} required for a given count-rate, and hence signal-to-noise ratio, is much higher for Kr. Expressed in terms of ΔP_{rad}/count-rate, the central-chord values are typically: for Ar 250 MHz/MW, for Fe 40 MHz/MW, and for Kr 1 MHz/MW. Also, the H-like spectrum is not complicated by blends of satellite lines from lower ionization stages, thereby simplifying reconstruction of radial profiles. A further advantage of Fe over similar-Z metals such as Ni, is that the relevant Fe wavelengths are very close to double those of Kr, making it possible to design a system that can observe both impurities with minimal adjustments. This coincidence has been exploited in a precision measurement of the He-like

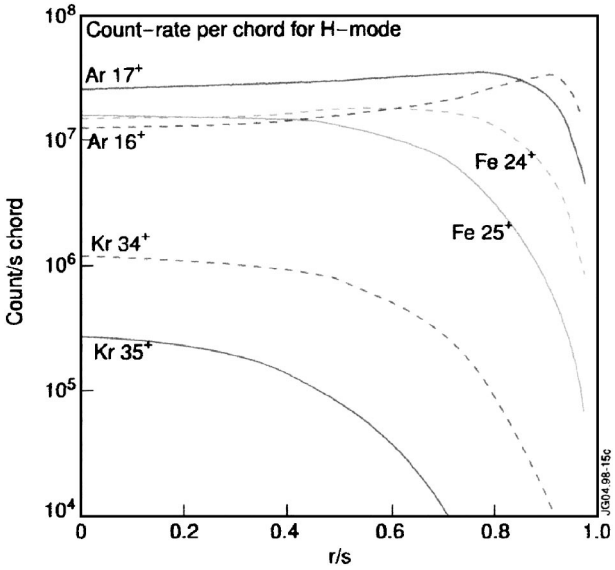

FIG. 5. Detector count-rate per chord for 35 channels.

Kr spectrum.[11] Most preceding ITER design studies have been based on Kr, but these results suggest that for the smaller plasma of ITER, the main reason to use Kr is for its easier introduction into the plasma, not its ionization balance, and that any of the metals in the Fe-Zn range would be preferable for core measurements if a consistent source could be achieved.

Good signal-to-noise ratios can be achieved with 100 ms integration time, for impurity radiated power less than 500 kW, the main contribution to the signal-to-noise being the plasma continuum radiation on which the lines are superimposed. The accompanying study[1] of the optimization of sight lines and profile reconstruction for the various spectral lines, shows that good radial coverage can be achieved with either Fe^{25+} or Kr^{34+} for the core and Ar^{17+} for the outer plasma, with considerable overlap, and that the ITER measurement requirements ($\delta a/a = 0.1$, $\delta t = 100$ ms) can be met.

ACKNOWLEDGMENTS

This work was carried out under a contract from the European Fusion Development Agreement and funded by the UK Engineering and Physical Sciences Research Council and EURATOM.

[1] C. Ingesson, Rev. Sci. Instrum., these proceedings.
[2] H. P. Summers, Available http://adas.phys.strath.ac.uk.
[3] L. Lauro-Taroni *et al.*, *Proceedings 21st EPS Conference Controlled Fusion and Plasma Physics*, Montpelier, 1.
[4] A. Loarte, EFDA-CSU, Garching, Germany.
[5] M. Bitter, Rev. Sci. Instrum., these proceedings.
[6] S. G. Lee, Rev. Sci. Instrum., these proceedings.
[7] G. Bertschinger, Rev. Sci. Instrum., these proceedings.
[8] M. Nelson, Rev. Sci. Instrum., these proceedings.
[9] K. W. Hill, Rev. Sci. Instrum., these proceedings.
[10] M. Bitter *et al.*, Phys. Rev. Lett. **71** (7), 1007 (1993).
[11] K. Widmann *et al.*, Phys. Rev. A **53** (4), 2200 (1996).
[12] R. Barnsley *et al.*, in *Diagnostics for Experimental Thermonuclear Fusion Reactors 2*, edited by Stott *et al.* (Plenum, New York, 1998), p. 307.
[13] P. H. Edmonds *et al.*, in *Diagnostics for Experimental Thermonuclear Fusion Reactors*, edited by Ed Stott *et al.* (Plenum, New York, 1998), 79.
[14] H. Lida, ITER-IT, Garching, Germany.
[15] U. Schumacher *et al.*, Rev. Sci. Instrum. **60**, 4, 562 (1989).
[16] R. Barnsley *et al.*, Rev. Sci. Instrum. **57**, 2159 (1986).
[17] R. Barnsley *et al.*, Rev. Sci. Instrum. **74**, 2388 (2003).
[18] I. Coffey, Rev. Sci. Instrum., these proceedings.